THE MECHANICS OF REINFORCEMENT IN POLYMER-BASED NANOCOMPOSITES

Robert J. Young[1], Ian A. Kinloch[2] and Dimitrios G. Papageorgiou[3]

[1] National Graphene Institute and School of Materials, The University of Manchester, Manchester, M13 9PL, UK, robert.young@manchester.ac.uk, http://www.graphene.manchester.ac.uk/discover/the-people/robert-j-young/
[2] National Graphene Institute and School of Materials, The University of Manchester, Manchester, M13 9PL, UK, ian.kinloch@manchester.ac.uk, http://www.graphene.manchester.ac.uk/discover/the-people/ian-kinloch/
[3] National Graphene Institute and School of Materials, The University of Manchester, Manchester, M13 9PL, UK, dimitrios.papageorgiou@manchester.ac.uk

Keywords: Graphene, Nanocomposites, Mechanics, Raman spectroscopy

ABSTRACT

A detailed analysis has been undertaken of the mechanisms of reinforcement of polypropylene (PP) by the addition of graphene nanoplatelets (GNP). The PP/GNP nanocomposites were processed by melt mixing followed by injection moulding and microstructure was fully characterized. The mechanical properties of the nanocomposites were evaluated using both tensile testing and dynamic mechanical thermal analysis. The addition of GNPs led to a significant increase in the Young's modulus of the PP, coupled with a decrease in the yield stress and a reduction in the elongation to failure. Stress transfer from the PP matrix to the GNP reinforcement was followed from stress-induced shifts of the 2D Raman band and the effective Young's modulus of the GNPs in the nanocomposites was found to be of the order of 100 GPa, shown to be consistent with the expected value.

1 INTRODUCTION

Graphene was first isolated by Novoselov, Geim and coworkers in Manchester in 2004 who demonstrated that individual one-atom thick graphene layers could be prepared by the mechanical cleavage of graphite using adhesive tape [1-3]. The discovery of the world's thinnest material with its remarkable electronic properties led to Novoselov and Geim being awarded the 2010 Nobel Prize for Physics [4, 5]. Researchers have shown particular interest in graphene because its sp^2 hybridized carbon atoms arranged in a honeycomb network structure displays considerable levels of stiffness and strength, close to the theoretical limit [6]. It was soon realised that the addition of graphene to a polymer matrix could result in a significant improvements in mechanical properties of the materials, particularly in stiffness and strength [7-17]. It was also thought that the addition of graphene could influence crystal nucleation and the microstructure of the nanocomposite [7]. Additionally, there are a number of different ways of processing the nanocomposites and they can influence the dispersion of graphene in nanocomposite and the subsequent physical properties [8-10]. Graphene-reinforced polymers are already being used in applications such as sporting goods [18, 19].

Young, Kinloch and coworkers [20, 21] have undertaken a number of studies of the fundamental mechanisms of reinforcement of polymers by graphene-based materials in model nanocomposites and have investigated the effect of the lateral dimensions of the graphene nanoplatelets [22, 23], the number of layers [24, 25], surface chemistry [26, 27] and orientation [28, 29]. It is found that these nanomaterials generally follow the rules of continuum mechanics formulated for macroscopic fibre-reinforced polymers [20]. Overall the best properties are predicted to be found for large, well-aligned, few-layer graphene nanoplatelets with good interfacial adhesion.

A number of studies have been undertaken to test these predictions for polymer matrix nanocomposites. For example, it was shown clearly that flakes with large lateral dimensions lead to higher values of Young's modulus than smaller flakes for a given volume fraction in a polypropylene matrix[30]. Stress transfer between graphene oxide (GO) nanoplatelets and a poly(vinyl acetate)

(PVA) matrix has been demonstrated to be more efficient for well-aligned GO nanoplatelets [29, 31]. Controlling the surface chemistry of graphene oxide in an epoxy matrix nanocomposite has also been shown to have a strong affect upon the mechanical properties of the material [32].

Graphene nanoplatelets have become widely available as a cost-effective filler for polymer-matrix nanocomposites [7, 8, 33]. Strictly speaking, such materials should be termed "graphite nanoplatelets" since they contain more than 10 graphene layers [33, 34] but the terminology "graphene nanoplatelets" (GNPs) adopted in other publications will be followed here. This present study is concerned with the effect of the addition of these graphene nanoplatelets to polypropylene (PP) upon the structure and mechanical properties of the material. Polypropylene (PP) is used widely due to its relatively low cost and being non-toxic and non-hazardous. The density of PP is low and it is essentially the lightest generally-used plastic. PP has good chemical stability, showing great resistance to both acids and alkalis and its bending fatigue resistance is also excellent. For specific applications, these properties of PP are usually impressive compared to the other plastics leading to it being used extensively in home appliances, as well as automotive and aerospace components.

In this presentation it will be shown how Raman spectroscopy can be employed to follow stress transfer from the PP matrix to GNPs in a PP/GNP nanocomposite, investigate the deformation micromechanics and so evaluate the efficiency of the GNP reinforcement. It will be demonstrated that it is possible to analyse the mechanical behaviour of these nanocomposites in terms of a modified rule of mixtures model, as opposed to the empirical approaches such as the Halpin-Tsai model, employed widely in previous studies [20].

2 EXPERIMENTAL

2.1 Materials

The graphene-based material employed was xGnP graphene nanoplatelets, Grade M with an average particle diameter of 15 µm, supplied by XG Sciences of Michigan, USA. The average thickness of Grade M GNP particles is 6 - 8 nm, with a surface area typically of about 120 - 150 m^2/g and a density of 2.2 g/cm^3 [33].

The polypropylene used was a commercial material, 100-CA50 nucleated polypropylene homopolymer, supplied by Ineos Olefins & Polymers Europe. The melt flow index (230 °C / 2.16 kg) of this polymer was given by the manufacturer as 50 g/10 min, its flexure modulus (ISO 178 at 23 °C) is 1.55 GPa and its density was quoted as 0.9 g/cm^3 [35].

2.2 Processing

Compounding of the nanocomposites was carried out in a HAAKE™ MiniLab II Micro Compounder using a temperature of 180 °C and a rotor speed of 50 rpm for 5 minutes for each sample. Pure PP was also prepared using the Haake Minilab mixing machine. The material was charged into the mixing chamber immediately after the motor started and was allowed to equilibrate for 5 minutes. For the PP/GNP composites, firstly, polypropylene was charged into the mixing chamber immediately after the motor started and was allowed to equilibrate for 3 minutes. The xGnP material was then added into the mixing chamber and the melt mixing was continued for further 2 minutes.

All raw materials were prepared and weighed according to the nominal formulations. The composite samples were then injection moulded using a Haake Minijet Injection Moulding Machine to produce dumbbell-shaped tensile specimens (ISO 527-2-1BA), with a thickness of 1.5 mm (as opposed > 2 mm specified in the standard). The injection moulding procedure was undertaken using a cylinder temperature of 200 °C, a mould temperature of 40 °C and a pressure of 400 bar for 10 s. The processing conditions employed were those normally used in our laboratory to process PP and were not optimised for the PP/GNP composites, as will be discussed later.

2.3 Scanning electron microscopy

In this study, the SEM images were obtained of the GNPs and from the nanocomposites using a Philips XL30 field emission gun scanning electron microscope (FEG SEM). The GNPs were dispersed

upon aluminium SEM stubs using a solvent. The samples of PP and nanocomposites were examined after cryogenic fracture following immersion in liquid nitrogen. The specimens were then mounted on stubs and sputter coated with a thin layer of Palladium (Pd) to avoid electrostatic charging during examination. The images of the different samples were obtained at a variety of magnifications

2.4 Raman spectroscopy

Raman spectra were obtained using a Renishaw 1000 Raman Spectrometer with an Olympus BH2-UMA microscope and a 514 nm argon ion laser. A spot size of between 1 and 2 μm was obtained using a ×50 magnification objective lens with a long working distance (LWD). The Raman system was calibrated using the 520 cm^{-1} band of silicon and spectra were obtained using 10% laser power, 10 s exposure time and 3 accumulations. Spectra were obtained from the GNP particles, the pure PP and the PP/GNP nanocomposites. The GNP nanoparticles were compressed by a glass cover slip to obtain a thin flat layer of GNPs on a glass slide. Spectra were obtained from moulded surfaces of the pure PP and the PP/GNP nanocomposites. The data were recorded and analysed using WIRE 3.3 and Origin 8.5 software and the curves were fitted using Lorentzian curve fitting procedures.

2.5 Tensile testing

Tensile test of composites was carried out according to ASTM D638 at 25 ± 3 °C and a cross head speed of 5 mm/min using an Instron Model 1121, Universal Testing Machine with Series IX software. In addition, an extensometer was used to follow changes in the length of specimens with the gauge length set at 5 mm. Stress-strain curves were obtained for each specimen tested. The tensile properties (modulus of elasticity, elongation at break and yield strength) were determined for 5 nominally-identical specimens for each composition using Origin 8.5 software and average values of each parameter are reported.

2.6 Raman deformation analysis

Stress transfer from the PP matrix to the GNPs was followed from shift with strain of the 2D Raman band of the GNPs in the nanocomposites. This was undertaken by bending 70 mm long bars of the nanocomposites around 1.5 mm thick in a Renishaw 1000 Raman Spectrometer with an Olympus BH2-UMA microscope and a 514 nm argon ion laser. The specimens were cut from the injection moulded dumbbells and deformed using a specially-designed four-point being rig placed on the microscope stage of the spectrometer. The strain on the tensile surface of the bars was determined using a resistance strain gauge glued to the surface of the bar adjacent to the region illuminated by the focussed laser spot.

3 RESULTS AND DISCUSSION

3.1 Scanning electron microscopy

Scanning electron microscopy was also employed to characterize the microstructure of the materials. Figure 1a shows the structure of the GNPs with an average diameter of around 15 μm. Figure 1b shows the cryo-fracture surface of the PP which is typical of that of a polymer that is ductile at ambient temperature. The fracture surface of the PP/GNP nanocomposite with the highest GNP loading of 5.2 vol% is shown in Figure 1c and is quite different from that of the neat PP. The edges of the GNPs can be seen on this fracture surface and it appears that they are well distributed and have maintained their lateral dimensions in the nanocomposite.

Kalaitzidou et al [7] found that poor dispersions were obtained at GNP loadings of the order of 10 vol% in PP, but it appears that a good dispersion has been maintained in our materials by using lower loadings.

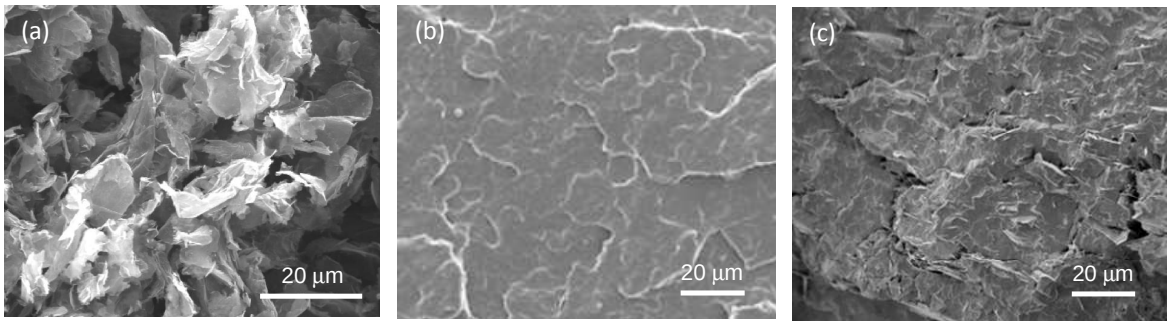

Figure 1: Scanning electron micrographs of (a) the GNP platelets, (b) a fracture surface of the PP and (c) a fracture surface of the PP/GNP nanocomposite with 5.2 vol% GNP loading.

3.2 Raman spectroscopy

The microstructure of the nanocomposites was also determined using Raman spectroscopy. A series of Raman spectra for the PP and the PP/GNP nanocomposites are presented in Figure 2. The spectrum for the neat PP in Figure 2 is relatively weak, showing only a number of strong bands around 3000 cm^{-1}. The Raman spectra for the nanocomposites are quite different with the D, G and 2D bands from the GNPs now present [21]. The intensity of these bands relative to the 3000 cm^{-1} bands of the PP matrix appears to show no systematic dependence upon the volume fraction of the GNP filler. This is because the Raman laser spot size is smaller than the lateral dimensions of the particles. No preferred orientation of the GNPs was found using polarized Raman spectroscopy upon sections taken in different directions [28, 29].

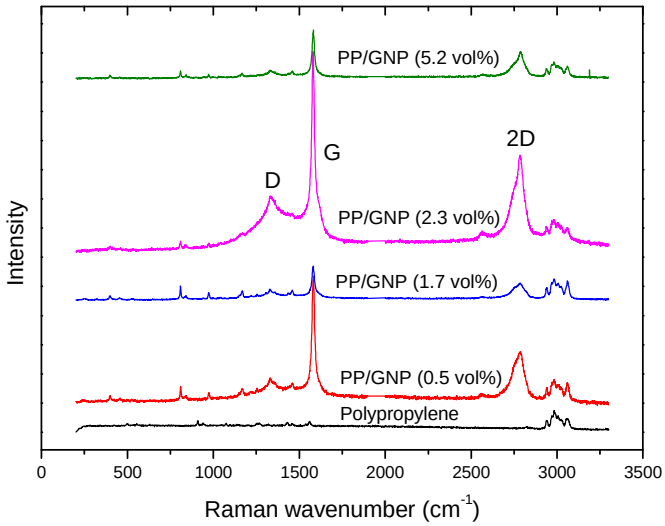

Figure 2: Raman spectra obtained from the PP and PP/GNP nanocomposites.

3.3 Tensile testing

Figure 3 shows the stress strain curves for PP/GNP nanocomposites for different levels of GNP loading. The stress-strain curves were used to determine the Young's modulus (initial slope in the elastic region of the graph), the elongation at break and the yield strength (the maximum stress before plastic deformation) of the nanocomposites. These data are shown in Figure 4. It can be seen from Figure 4 that there is a significant increase in the stiffness of the PP upon the addition of the GNPs and that the Young's modulus increases from around 1.3 GPa to over 2.0 GPa, as has been found before [30]. At the same time there is an embrittlement of the material with the fracture strain decreasing from more than 250% to less than 10% at the highest loadings of GNPs. In addition there is a slight reduction of the yield stress of the PP (defined as the peak stress in the stress-strain curve) from around 34 MPa to just over 30 MPa due probably to poor adhesion between the GNPs and PP.

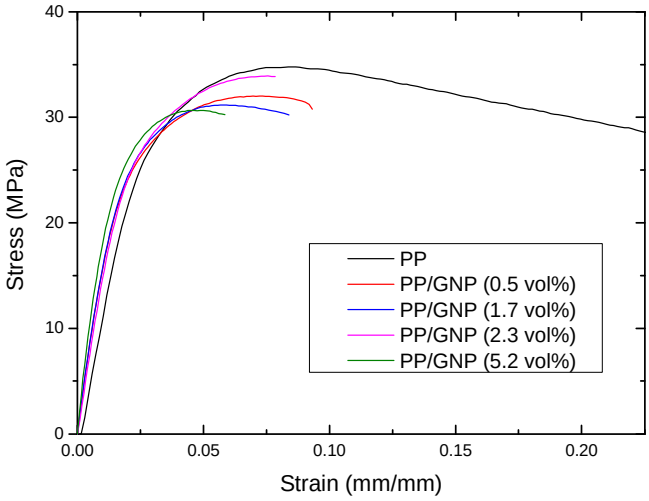

Figure 3: Stress-strain curves for the PP and PP/GNP nanocomposites as a function of GNP loading.

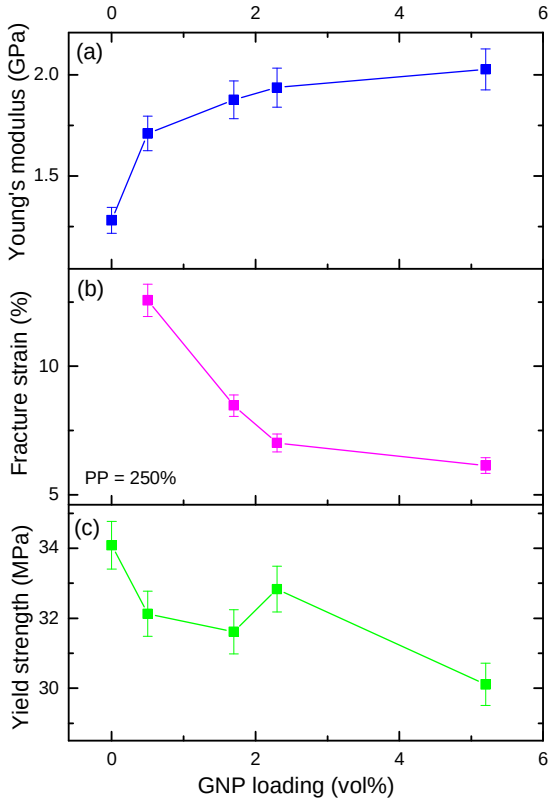

Figure 4: Variation of (a) the Young's modulus, (b) the fracture strain and (c) the yield strength of the PP/GNP nanocomposites as a function of GNP loading.

3.4 Raman deformation analysis

It is well established that stress transfer from a polymer matrix to a graphene-based reinforcement can be followed from stress-induced Raman band shifts in the graphene phase [20-23, 25]. Figure 5 shows the dependence upon strain of the position of the 2D Raman band in the different nanocomposites fitted to a single Lorentzian function. There is a significant band shift for all the materials and it can be seen that the rate of shift determined from the slope of the lines is similar for all the materials and independent of the composition, within the scatter in the data.

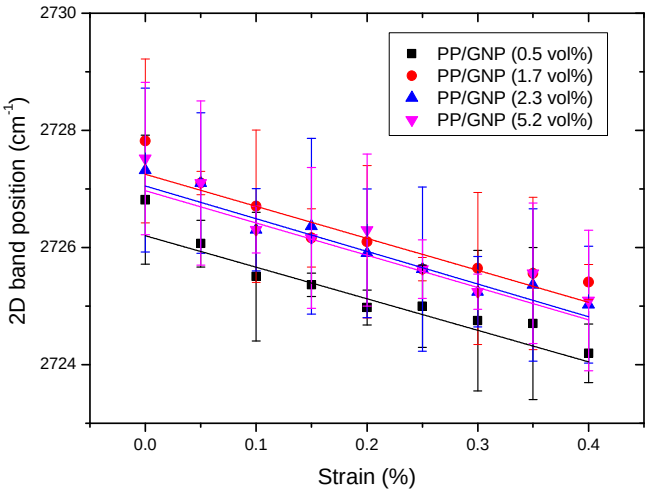

Figure 5: Dependence of the position of the 2D Raman bands in the PP/GNP nanocomposites on strain.

4 MECHANISMS OF STRESS TRANSFER

It is clear that the addition of the GNPs to the polypropylene modifies its mechanical properties significantly. Of most interest is the increase in Young's modulus shown in Figure 4. There are a number of ways in which this can be modelled but the simplest one is to use the rule of mixtures [35] which for a particulate- or platelet-reinforced composite can be expressed as

$$E_c = \varphi_p E_p + (1 - \varphi_p) E_m \quad (1)$$

where E_c, E_p and E_m are the Young's moduli of the composite, particles (or platelets) and matrix and φ_p is the volume fraction of the particles. This equation assumes a state of uniform strain in the composites, i.e. the strain in the reinforcement is that same as the strain in the matrix. In the case of the PP/GNP nanocomposites the effective Young's modulus of the GNP nanoparticles, E_{eff} ($\equiv E_p$), in the nanocomposites can be determined using Equation 1 from the measured values of E_c, E_m and φ_p. The values of E_{eff} are listed in Table 1 derived from the data for both the Young's modulus and storage modulus determined from dynamic mechanical thermal analysis (DMTA) are reported elsewhere [36].

The effective Young's modulus of the reinforcement can be determined independently from the shift of the 2D Raman band shown in Figure 5. It is well established that the rate of shift of the 2D Raman band in monolayer graphene with a Young's modulus of 1050 GPa is around -60 cm^{-1}/% strain. This relationship can be used to estimate the Young's modulus of a range of difference sp^2 carbon materials [37] including carbon nanotubes [38, 39], few-layer graphene [24], graphene oxide [29, 31] and carbon fibres [40]. For example, a material that exhibits a band shift rate of -5.5 cm^{-1}/% strain has an effective Young's modulus of 1050 × 5.5/60 = 96.25 GPa. The values of E_{eff} estimated for the GNPs in the nanocomposites from the Raman band shift data are also given in Table 1.

GNP loading	Effective Young's Modulus of the GNPs (E_{eff})		
vol%	Tensile	DMTA	Raman
0.5	84 ± 25	97 ± 5	94.5 ± 3.5
1.7	36.0 ± 7.1	41.4± 3.6	94.5 ± 3.5
2.3	26.6 ± 5.3	47.3 ± 1.7	98.0 ± 3.5
5.2	13.6 ± 2.3	21.9 ± 1.6	96.2 ± 3.5

Table 1: Values of the effective Young's modulus of the GNP reinforcement determined using the different experimental techniques.

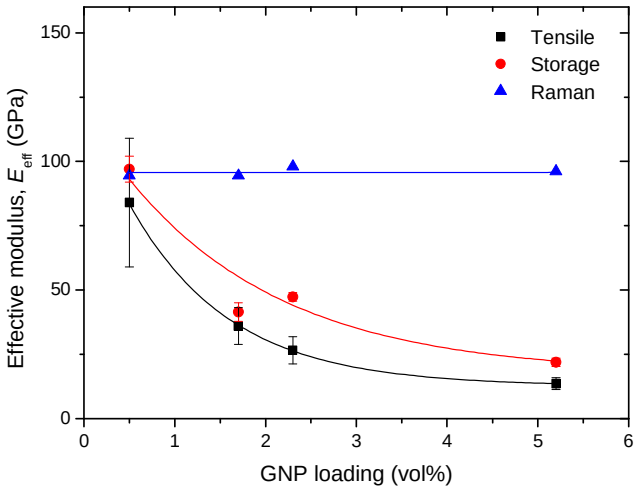

Figure 6: Dependence of the effective modulus of the GNP reinforcement in the PP/GNP nanocomposites, determined from the different experimental measurements, upon GNP loading.

Figure 6 summarizes the dependence of the effective modulus of the GNP reinforcement in the nanocomposites upon the GNP loading. It can be seen that the values determined from the Raman 2D band shift data are independent of the GNP loading whereas the values determined from the measured Young's modulus and storage modulus decrease as the GNP loading increases. Although this difference in behaviour with GNP loading may appear to be an anomaly, it is the direct consequence of the state of uniform strain in the nanocomposites. Young and Eichhorn [41] reviewed the use of Raman spectroscopy to follow the micromechanics of deformation in composites and showed that for a system in which there was uniform strain, it would be expected that the Raman band shift rate with *strain* would be independent of volume fraction of the reinforcement. On the other had the Raman band shift rate with *stress* should depend on the volume fraction [41]. Our present measurements in Figure 6 are for the rate of shift with *strain* and Equation 1 also assumes uniform strain.

It is found that all the derived values of E_{eff} converge as the GNP loading approaches zero to a value of around 100 GPa. The Young's modulus was determined from measurements on the bulk nanocomposites whereas the Raman band shifts were determined from a 1-2 μm region that is smaller than the individual GNP flake size – essentially from the deformation of individual flakes and so independent of the level of GNP loading in the situation of uniform strain. On the other hand, the measurements on the bulk polymer will evaluate the mechanical behaviour of the whole nanocomposites and be sensitive to factors such as interactions between nanoparticles and possible restacking effects that disappear at low volume fractions.

5 CONCLUSIONS

It is clear that the addition of graphene nanoplatelets to polypropylene to form PP/GNP nanocomposites leads to a major modification of the mechanical properties of the polymer. It is found that the Young's modulus of the PP/GNP nanocomposites increases with the loading of the GNPs and the effective Young's modulus of the reinforcement is found from mechanical testing to be of the order of 100 GPa, consistent with that expected for the GNPs, taking into account the number of graphene layers in the nanoplatelets, their random orientation and finite length. Raman spectroscopy has been employed to both characterise the microstructure of the nanocomposites and follow stress transfer from the PP matrix to the GNP reinforcement from stress-induced shifts of the 2D Raman band. The shift of the band per unit strain enabled the effective Young's modulus of the GNP reinforcement to be determined and this was again found to be of the order of 100 GPa, consistent with the value determined from mechanical testing. It should be pointed out that the nanocomposite system investigated in this present study is far from being optimised. A nucleated PP homopolymer matrix has been employed and it would be of interest to investigate the effect of using other forms of PP. Only one size of unfunctionalized GNPs has been used and better performance may be obtained with

different particle sizes and functionalized GNPs. Again only one set of mixing processing conditions has been employed and different conditions may lead to better particle dispersions.

ACKNOWLEDGEMENTS

The authors are grateful to Siti Rohana Ahmad and Chengzhe Xue for undertaking much of the experimental work reported in this study.

REFERENCES

[1] A.K. Geim, Graphene: Status and prospects, *Science*, **324**, 2009, pp 1530-1534.
[2] A.K. Geim, K.S. Novoselov, The rise of graphene, *Nature Materials*, **6**, 2007, pp 183-191.
[3] K.S. Novoselov, A.K. Geim, S.V. Morozov, D. Jiang, Y. Zhang, S.V. Dubonos, I.V. Grigorieva, A.A. Firsov, Electric Field Effect in Atomically Thin Carbon Films, *Science*, **306**, 2004, pp 666-669.
[4] A.K. Geim, Random Walk to Graphene, *International Journal of Modern Physics B*, **25**, 2011, pp 4055-4080.
[5] K.S. Novoselov, Graphene: Materials in the Flatland, *International Journal of Modern Physics B*, **25**, 2011, pp 4081-4106.
[6] C. Lee, X. Wei, J.W. Kysar, J. Hone, Measurement of the Elastic Properties and Intrinsic Strength of Monolayer Graphene, *Science*, **321**, 2008, pp 385-388.
[7] K. Kalaitzidou, H. Fukushima, P. Askeland, L.T. Drzal, The nucleating effect of exfoliated graphite nanoplatelets and their influence on the crystal structure and electrical conductivity of polypropylene nanocomposites, *Journal of Materials Science*, **43**, 2008, pp 2895-2907.
[8] K. Kalaitzidou, H. Fukushima, L.T. Drzal, A new compounding method for exfoliated graphite–polypropylene nanocomposites with enhanced flexural properties and lower percolation threshold, *Composites Science and Technology*, **67**, 2007, pp 2045-2051.
[9] M. El Achaby, F.-E. Arrakhiz, S. Vaudreuil, A. El Kacem Qaiss, M. Bousmina, O. Fassi-Fehri, Mechanical, thermal, and rheological properties of graphene-based polypropylene nanocomposites prepared by melt mixing, *Polymer Composites*, **33**, 2012, pp 733-744.
[10] M. El Achaby, A. Qaiss, Processing and properties of polyethylene reinforced by graphene nanosheets and carbon nanotubes, *Materials & Design*, **44**, 2013, pp 81-89.
[11] X. Jiang, L.T. Drzal, Multifunctional high-density polyethylene nanocomposites produced by incorporation of exfoliated graphene nanoplatelets 2: Crystallization, thermal and electrical properties, *Polymer Composites*, **33**, 2012, pp 636-642.
[12] I.-H. Kim, Y.G. Jeong, Polylactide/exfoliated graphite nanocomposites with enhanced thermal stability, mechanical modulus, and electrical conductivity, *Journal of Polymer Science Part B: Polymer Physics*, **48**, 2010, pp 850-858.
[13] S. Kim, I. Do, L.T. Drzal, Thermal stability and dynamic mechanical behavior of exfoliated graphite nanoplatelets-LLDPE nanocomposites, *Polymer Composites*, **31**, 2009, pp 755-761.
[14] J.R. Potts, D.R. Dreyer, C.W. Bielawski, R.S. Ruoff, Graphene-based polymer nanocomposites, *Polymer*, **52**, 2011, pp 5-25.
[15] P. Song, Z. Cao, Y. Cai, L. Zhao, Z. Fang, S. Fu, Fabrication of exfoliated graphene-based polypropylene nanocomposites with enhanced mechanical and thermal properties, *Polymer*, **52**, 2011, pp 4001-4010.
[16] A. Yasmin, I.M. Daniel, Mechanical and thermal properties of graphite platelet/epoxy composites, *Polymer*, **45**, 2004, pp 8211-8219.
[17] M.A. Milani, D. González, R. Quijada, N.R.S. Basso, M.L. Cerrada, D.S. Azambuja, G.B. Galland, Polypropylene/graphene nanosheet nanocomposites by in situ polymerization: Synthesis, characterization and fundamental properties, *Composites Science and Technology*, **84**, 2013, pp 1-7.
[18] HEAD Technology Ltd, Sporting Goods with Graphene Material, in: U.S.P. Office (Ed.) HEAD Technology GMBH, Ltd, USA, 2013, p. 4.
[19] R.J. Young, L. Mufeng, The microstructure of a graphene-reinforced tennis racquet, *Journal of Materials Science*, **51**, 2016, pp 3861-3867.

[20] R.J. Young, I.A. Kinloch, L. Gong, K.S. Novoselov, The mechanics of graphene nanocomposites: a review, *Composites Science and Technology*, **72**, 2012, pp 1459-1476.
[21] R.J. Young, I.A. Kinloch, Graphene and graphene-based nanocomposites, *Nanoscience, Vol 1: Nanostructures through Chemistry*, **1**, 2013, pp 145-179.
[22] L. Gong, I.A. Kinloch, R.J. Young, I. Riaz, R. Jalil, K.S. Novoselov, Interfacial Stress Transfer in a Graphene Monolayer Nanocomposite, *Advanced Materials*, **22**, 2010, pp 2694-2697.
[23] R.J. Young, L. Gong, I.A. Kinloch, I. Riaz, R. Jalil, K.S. Novoselov, Strain Mapping in a Graphene Monolayer Nanocomposite, *ACS Nano*, **5**, 2011, pp 3079-3084.
[24] L. Gong, R.J. Young, I.A. Kinloch, I. Riaz, R. Jalil, K.S. Novoselov, Optimizing the Reinforcement of Polymer-Based Nanocomposites by Graphene, *ASC Nano*, **6**, 2012, pp 2086-2095.
[25] L. Gong, R.J. Young, I.A. Kinloch, S.J. Haigh, J.H. Warner, J.A. Hinks, Z. Xu, L. Li, F. Ding, I. Riaz, R. Jalil, K.S. Novoselov, Reversible Loss of Bernal Stacking during the Deformation of Few-Layer Graphene in Nanocomposites, *ACS Nano*, **7**, 2013, pp 7287-7294.
[26] Z. Li, R. Wang, R.J. Young, L. Deng, F. Yang, L. Hao, W. Jiao, W. Liu, Control of the functionality of graphene oxide for its application in epoxy nanocomposites, *Polymer*, **54**, 2013, pp 6437-6446.
[27] Z. Li, R.J. Young, R. Wang, F. Yang, L. Hao, W. Jiao, W. Liu, The role of functional groups on graphene oxide in epoxy nanocomposites, *Polymer*, **54**, 2013, pp 5821-5829.
[28] Z.L. Li, R.J. Young, I.A. Kinloch, N.R. Wilson, A.J. Marsden, A.P.A. Raju, Quantitative determination of the spatial orientation of graphene by polarized Raman spectroscopy, *Carbon*, **88**, 2015, pp 215-224.
[29] Z.L. Li, R.J. Young, N.R. Wilson, I.A. Kinloch, C. Vallés, Z. Li, The Effect of the Orientation of Graphene-Based Nanoplatelets upon their Ability to Reinforce Composites, *Composites Science and Technology*, **123**, 2016, pp 125-133.
[30] C. Valles, A.M. Abdelkader, R.J. Young, I.A. Kinloch, Few layer graphene–polypropylene nanocomposites: the role of flake diameter, *Faraday Discussions*, **173**, 2014, pp 379-390.
[31] Z. Li, R.J. Young, I.A. Kinloch, Interfacial Stress Transfer in Graphene Oxide Nanocomposites, *ACS Applied Materials & Interfaces*, **5**, 2013, pp 456-463.
[32] C. Valles, F. Beckert, L. Burk, R. Mulhaupt, R.J. Young, I.A. Kinloch, Effect of the C/O Ratio in Graphene Oxide Materials on the Reinforcement of Epoxy-Based Nanocomposites, *Journal of Polymer Science Part B-Polymer Physics*, **54**, 2016, pp 281-291.
[33] XG Sciences, Technical Data Sheet xGnP Graphene Nanoplatelets- Grade M 2012.
[34] P. Wick, A.E. Louw-Gaume, M. Kucki, H.F. Krug, K. Kostarelos, B. Fadeel, K.A. Dawson, A. Salvati, E. Vazquez, L. Ballerini, M. Tretiach, F. Benfenati, E. Flahaut, L. Gauthier, M. Prato, A. Bianco, Classification Framework for Graphene-Based Materials, *Angewandte Chemie-International Edition*, **53**, 2014, pp 7714-7718.
[35] R.J. Young, P.A. Lovell, *Introduction to Polymers*, Third Edition, CRC Press, Boca Baton, Florida, USA, 2013.
[36] S.R. Ahmad, C.-Z. Xue, R.J. Young, The mechanisms of reinforcement of polypropylene by graphene nanoplatelets, *Materials Science and Engineering: B*, **216**, 2017, pp 2-9.
[37] O. Frank, G. Tsoukleri, I. Riaz, K. Papagelis, J. Parthenios, A.C. Ferrari, A.K. Geim, K.S. Novoselov, C. Galiotis, Development of a universal stress sensor for graphene and carbon fibres, *Nature Communications*, **2**, 2011, pp 255.
[38] C.A. Cooper, R.J. Young, M. Halsall, Investigation into the deformation of carbon nanotubes and their composites through the use of Raman spectroscopy, *Composites Part A: Applied Science and Manufacturing*, **32**, 2001, pp 401-411.
[39] L.B. Deng, S.J. Eichhorn, C.C. Kao, R.J. Young, The Effective Young's Modulus of Carbon Nanotubes in Composites, *ACS Applied Materials & Interfaces*, **3**, 2011, pp 433-440.
[40] R.J. Young, Monitoring deformation processes in high-performance fibres using Raman spectroscopy, *Journal of the Textile Institute*, **86**, 1995, pp 360-381.
[41] R.J. Young, S.J. Eichhorn, Deformation mechanisms in polymer fibres and nanocomposites, *Polymer*, **48**, 2007, pp 2-18.